Development of ΔE-E telescope ERDA with 40MeV 35Cl7+ beam at MALT in the University of Tokyo optimized for analysis of metal oxynitride thin films

doi: 10.1016/j.nimb.2016.07.019

Development of ΔE-E telescope ERDA with 40 MeV $^{35}Cl^{7+}$ beam at MALT in the University of Tokyo optimized for analysis of metal oxynitride thin films

I. Harayama[(1)], K. Nagashima[(1)], Y. Hirose[(2,3)], H. Matsuzaki[(4)], D. Sekiba[(1,5)]

[(1)]*Graduate School of Pure and Applied Sciences, University of Tsukuba, Tennoudai 1-1-1, Tsukuba Ibaraki 305-8573, Japan*

[(2)]*Graduate School of Science, The University of Tokyo, 7-3-1 Hongo, Bunkyo-ku Tokyo 113-0033, Japan*

[(3)]*CREST, Japan Science and Technology Agency, 7-3-1 Hongo, Bunkyo-ku, Tokyo 113-0033, Japan*

[(4)]*School of Engineering, The University of Tokyo, 7-3-1 Hongo, Bunkyo-ku Tokyo 113-8656, Japan*

[(5)]*Tandem Accelerator Complex, University of Tsukuba, Tennodai 1-1-1, Tsukuba Ibaraki 305-8577, Japan*

Abstract

We have developed a compact ΔE-E telescope elastic recoil detection analysis (ERDA) system, for the first time at Micro Analysis Laboratory, Tandem Accelerator (MALT) in the University of Tokyo, which consists of a gas ionization chamber and solid state detector (SSD) for the quantitative analysis of light elements. The gas ionization chamber is designed to identify the recoils of O and N from metal oxynitrides thin films irradiated with 40 MeV $^{35}Cl^{7+}$. The length of the electrodes along the beam direction is 50 mm optimized to sufficiently separate energy loss of O and N recoils in P10 gas at 6.0×10^3 Pa. The performance of the gas ionization chamber was examined by comparing the ERDA results on the $SrTaO_2N$ thin films with semi-empirical simulation and the chemical compositions previously determined by nuclear reaction analysis (NRA) and Rutherford backscattering spectrometry (RBS). We also confirmed availability of the gas ionization chamber for identifying not only the recoils of O and N but also those of lithium, carbon and fluorine.

1. Introduction

Recently the studies on partial replacement of anions in metal oxides or metal nitrides have been intensively performed. The continuous control of anion composition, such as O/N, in for example InO_xN_y [1] and $Sn{:}InO_xN_y$ (ITON)[2] enables us to tailor their optical, electronic and structural properties. In these studies, the determination of the elemental compositions in the synthesized samples is important, while the measurement and analysis are not straightforward when the samples are thin films and include multiple light elements. The combinations of typical methods in ion beam analysis, such as nuclear reaction analysis (NRA), Rutherford backscattering spectrometry (RBS) and elastic recoil detection analysis (ERDA) are good solutions of this problem. The comparison of the performances among various ion beam techniques

on ultra-thin AlO_xN_y films is well summarized by Barradas *et al.* [3] In previous works, we applied NRA of $^{15}N(p, \alpha\gamma)^{12}C$ to estimate the nitrogen amount in oxynitride thin films such as anatase TaO_xN_y [4] and perovskite $SrTaO_xN_y$ [5].

ERDA is one of the most powerful techniques to determine the elemental composition of thin films including the light elements. ERDA with relatively heavy ions is often equipped with a system of the particle identification. One example is the combination of time-of-flight (TOF) and particle energy detection, so-called TOF-*E* ERDA. The applications of TOF-*E* ERDA for perovskite $LaTiO_xN_y$ are found in references [6,7]. Recently, the performance of the particle identification of TOF-*E* ERDA has been intensively improved, so that one can distinguish also the light metals in thin films [8-11], meanwhile the system has become rather sophisticated and expensive. Another choice for the particle identification is the conventional ΔE-*E* telescope ERDA system equipped with a gas ionization chamber [12]. As long as we concentrate our attention into the determination of O and N ratio in the metal oxynitrides, the conventional ΔE-*E* telescope ERDA is still useful. Because the detection system is small and simple, it is easy to increase the effective solid angle of the detector.

In this paper, we report our recent development of the ΔE-*E* telescope ERDA system, which is optimized to separate the recoils of O and N included in metal oxynitrides thin films. This is a development of ΔE-*E* telescope ERDA for the first time in Micro Analysis Laboratory, Tandem Accelerator (MALT) in the University of Tokyo. In the development, we referred the design of the gas ionization chamber for the accelerator mass spectrometry (AMS) of ^{10}Be and ^{26}Al [13]. The developed system worked well to determine the compositional ratio of N, O, and metals (cations) in films by tuning the lengths of electrodes and the gas pressure. Some applications of the developed system were previously published on the amorphous AlN_x [14], epitaxial InO_xF_y [15], and epitaxial CoO_xN_y [16] thin films.

2. Experimentals

2.1. Setup of scattering chamber and beam

The primary aim of development is the composition determination of O and N in the metal oxynitrides by means of the simultaneous ERDA and RBS. Figure 1 shows the experimental setup of the scattering chamber. The incident angle of the $^{35}Cl^{7+}$ beam is set at the angle of 75° from the surface normal of the samples. The recoils and backscattered particles are collected at 30° and 150° from the beam incident direction,

respectively. RBS was taken by a conventional solid state detector (SSD, ORTEC U-012-050-100), while ERDA was carried out with the combination of the gas ionization chamber and the SSD (ORTEC U-016-300-100).

The incident beam was chosen from the viewpoint of the intermediate mass between the light elements (C, N, O or F) and the transition metals, so that Al, Si and/or Cl were desirable candidates. In the actual measurements, ^{35}Cl was used with the pressed NaCl target as an ion source cathode. The cation/anion ratio in the samples can be determined by means of the solid angle ratio of RBS and ERDA detectors and also the scattering and recoil cross sections. We note that our samples often include heavy cations, such as In and Ta. In RBS between heavy incident ions (in our case $^{35}Cl^{7+}$) and heavy targets, the screening effect on the cross section due to the electronic screening in inner shells should be considered [17]. In the cases between ^{35}Cl and ^{181}Ta, the beam energy > 30 MeV is required to suppress the deviation of the cross section from the Rutherford cross section below 1%. Thus, the $^{35}Cl^{7+}$ ion was accelerated up to ~ 40 MeV by the electrostatic tandem accelerator (5 UD Pelletron by National Electrostatic Corporation) in MALT. The typical $^{35}Cl^{7+}$ beam size and current were 1 × 1 mm^2 shaped by a slit system and a few tens nA, respectively. The typical data acquisition time for the metal oxynitrides thin films in the previous reports [15,16] was from half an hour to one hour.

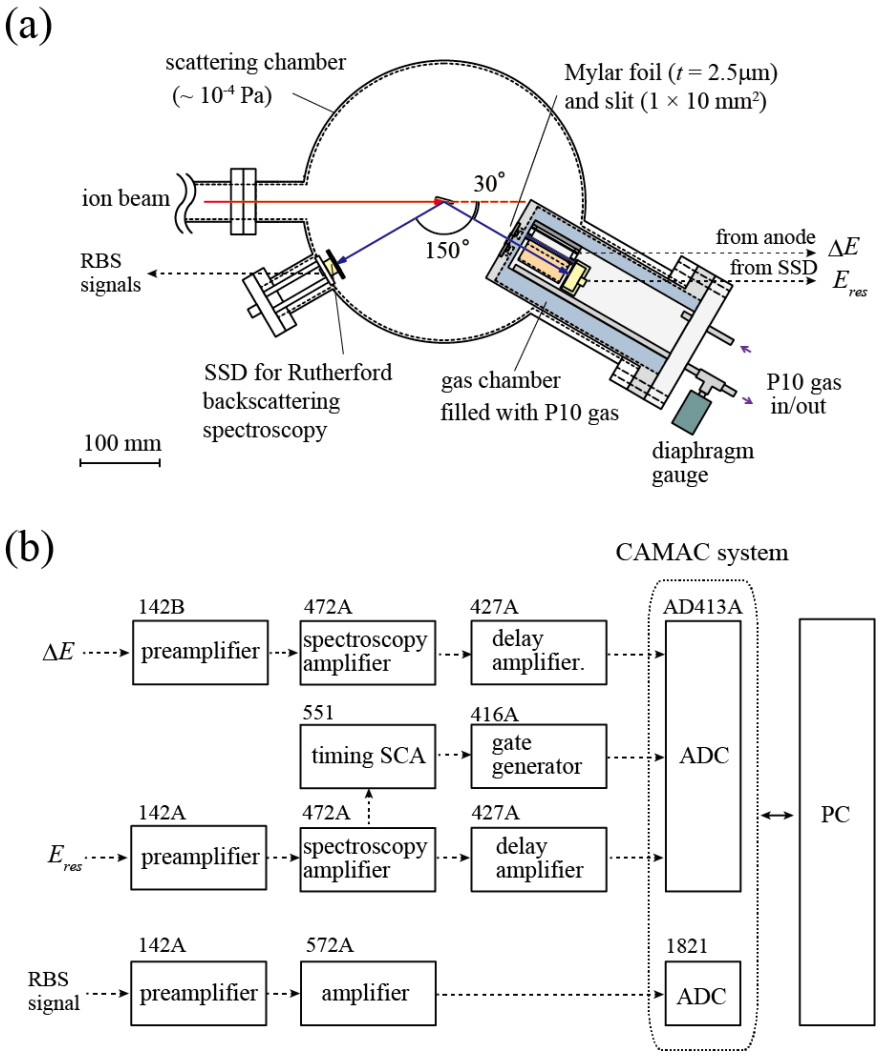

Fig. 1. (a) Schematics of scattering chamber setup equipped with the ΔE-E telescope ERDA and the RBS detectors. (b) The setup of the electronics system for the ΔE-E telescope ERDA and RBS. The number notated beside the electronics model number of ORTEC productions.

2.2 Design of gas ionization chamber

As mentioned above the U-shaped cathode (see Fig. 2(a)) in the gas ionization chamber adopted in the present study is a modification of that for AMS [13]. In principle, we did not change the cross section shape and dimensions of the gas ionization chamber from the original one. Here we discussed the length of electrodes along the recoil incident direction to separate N and O in the ΔE-E histogram. Assuming that the typical energy resolution of gas ionization chambers is ~ 100 keV, the difference of the energy loss in the gas ionization chamber between N and O ($\Delta E_O - \Delta E_N$) should be larger enough than the energy resolution. The P10 gas (90% Ar + 10% CH_4) is used to fill our

gas ionization chamber. The pressure of the P10 gas in the gas ionization chamber was measured with a diaphragm gauge at the outlet of the gas flow system (see Fig. 1). The P10 gas and/or Q gas (98% He + 2% isobutene) are easily available in our facility, and the Ar-based would be expected to make the gas ionization chamber more compact for the simple purpose to distinguish O and N. The energies of recoils of O and N from the sample surface by means of the 40 MeV $^{35}Cl^{7+}$ beam are 25.84 MeV and 24.49 MeV, respectively with the setup above. When the pressure of P10 gas is ~ 6.0×10^3 Pa, the stopping powers of the P10 gas for the above two recoils are 48.35 keV/mm and 39.25 keV/mm, respectively [18]. From these values, it is revealed that the electrode length of 50 mm induces a sufficient energy loss difference, $\Delta E_O - \Delta E_N \sim 450$ keV. The whole detection system of ΔE-E telescope ERDA is mounted on an ICF152 flange with the gas flow system, and the inlet of the detector is sealed with a Mylar foil (t = 2.5 μm). The slit shape of the detector inlet is 1 × 10 mm², so that the recoil angle is limited within 30° ± 0.35°. The distance between the sample and the slit is ~ 80 mm meaning that the solid angle of the telescope is ~ 1.5×10^{-3} sr. This solid angle is fully covered with the SSD of about 20 mm diameter. In the present development and study, the electrical voltages put on the anode (V_A), grid (V_G), and cathode (V_C) were the same to those adopted in AMS [13], i.e. V_A = 180 V, V_G = 30 V and V_C = 0 V (grounded as well as the vacuum chamber). A photograph of the developed system on the ICF152 flange is displayed in Fig. 2(b).

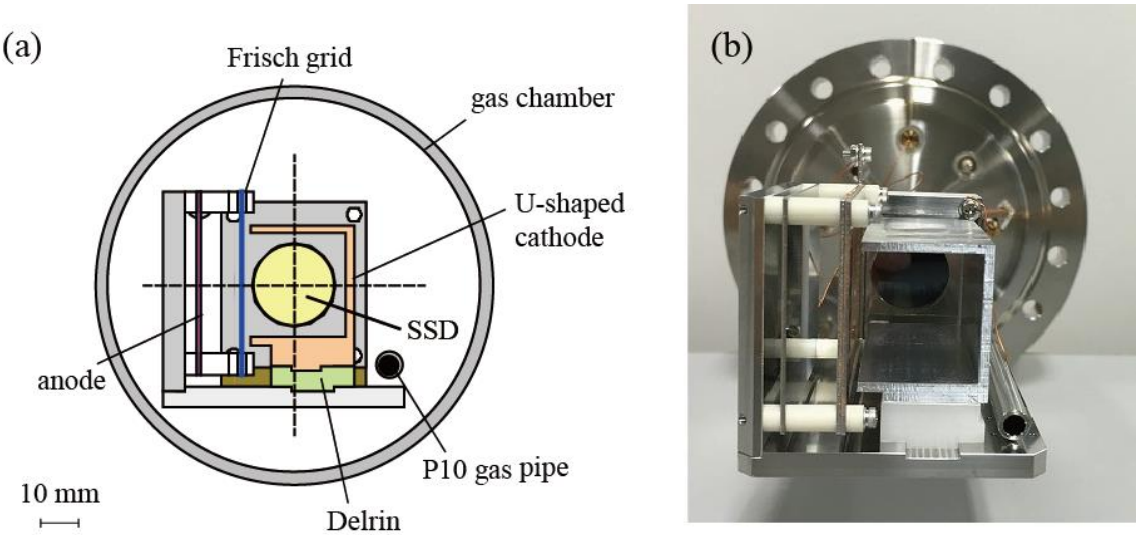

Fig. 2. (a) Schematics of the cross section of the ΔE-E telescope ERDA detector with the U-shaped cathode. (b) A photograph of the gas ionization chamber seen from the front.

2.3. Samples

For the energy calibration of the gas ionization chamber and the SSD, ^{16}O beam was used with sweeping the accelerated energy from ~ 19 up to ~ 25 MeV. An Au foil (t = 25 μm) was used as a target and the ^{16}O particles Rutherford (forward) scattered from the foil were collected by the same ΔE-E telescope system.

The performance of the developed gas ionization chamber for the elementary composition determination was checked on the $SrTaO_2N$ films (t = 60 and 100 nm) on the $SrTiO_3$ substrate. These $SrTaO_2N$ films were prepared with the established recipe, of which the stoichiometry was proved by RBS, NRA and the charge neutralized condition in the previous study [5].

Apart from above, the developed gas ionization chamber was applied for ΔE-E telescope ERDA on other metal oxides, oxynitrides, and oxyfluorides : the CoO_xN_y film (t = 90 nm) [16] on the $MgAl_2O_4$ substrate, the thick $LiTaO_3$ plate, an InO_xF_y film (t = 125 nm) on the Y:ZrO_2 substrate and the SiO_2 film (t = 47 nm) on the Si wafer.

3. Results and discussions

3.1. Response of detectors for swift light elements

We followed the procedure to obtain the coefficients converting the analog to digital converter (ADC) output to the energies of particles detected by the gas ionization chamber ΔE and by the SSD, so-called the residual energy E_{res}. E_{res} and ΔE are connected by the energy of recoils, so-called total energy E_{total}, as $E_{total} = \Delta E + E_{res} + E_{others}$. Here E_{others} represents the energy losses not directly measured by the detectors such as energy loss due to the Mylar foil at the inlet of the detection system and P10 gas out of electrodes. While we made the energy calibration carefully for E_{res} by the SSD, we roughly checked ΔE only for a typical energy of ^{16}O. In principle, it is not necessary to know E_{total} exactly, because the contributions of ΔE and E_{others} are just the shift of origin of energy scale in the interested energy region. This convenience can be rationalized by the two facts that (1) ΔE is not so sensitive to the kinetic energy of the light element recoils in this energy region and also (2) the interested energy region is narrow due to the small thickness of the films on the substrates. The specific discussion is given in the next subsection.

Figure 3(a) shows the ADC output of the SSD (E_{res}) put behind the gas ionization chamber (see Fig. 1 and 2) in the ΔE-E telescope ERDA system without the P10 gas. The ^{16}O particle forward scattered from the Au foil was detected through the Mylar foil at the inlet of the detection system with sweeping the acceleration energy of the ^{16}O beam. We can see that the output of the SSD can be well fitted by a linear function as $y = ax + b$, here a and b were determined as 253 ch/MeV and -1029 ch. Where

"ch" signifies the channel of the ADC output, while the above calibrated value of course can linearly depend on the amplifier gain in the electronics. The *y*-intercept (or *x*-intercept more directly in the dimension of energy) corresponds mainly to the energy loss due to the Mylar foil at the inlet. According to the stopping power of Mylar foil against ^{16}O with the energy around ~ 22 MeV [18], the thickness of the Mylar foil was estimated as ~ 3.5 μm, while we used the film with the thickness of 2.5 μm. The discrepancy is not significant for our purpose and will be interpreted by the fluctuation of density or carbon pile up, etc. Now we obtain the energy calibration factor 1/a = 3.95 keV/ch for the SSD in the ΔE-E telescope ERDA system. Hereafter we assume, for the simplification, that the responses of the SSD for the swift ^{14}N and other light elements are approximately same to that for ^{16}O. The elementary dependence of the SSD response [19] should be, however, taken into account in the case that the precise depth distribution is required.

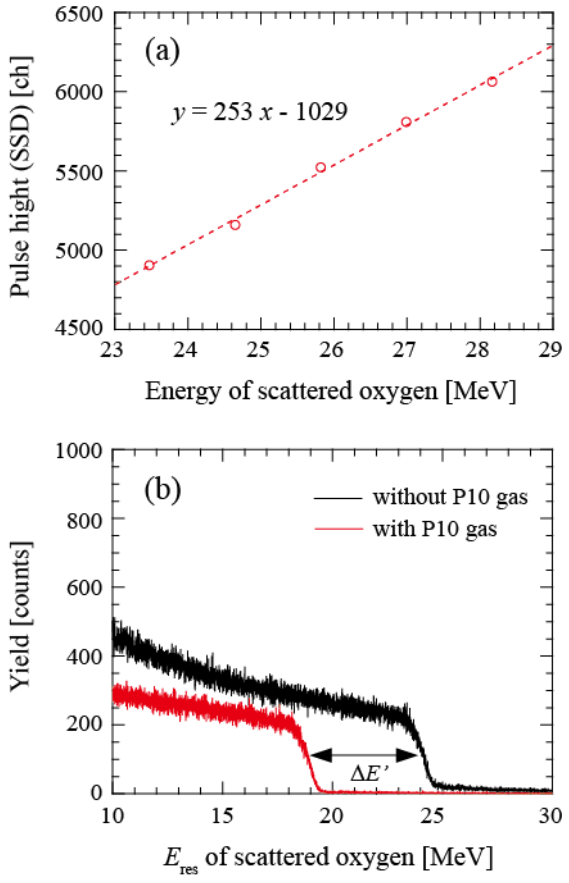

Fig. 3. (a) Observed pulse height of the SSD output as a function of the energy of ^{16}O scattered from the Au target. (b) Spectra of ^{16}O scattered from the Au target taken by the SSD without (black line) and with (red line) P10 gas.

Then we now give a rough discussion on the response of the gas ionization

chamber for swift ions of the light elements. Figure 3(b) shows the energy spectra of ^{16}O scattered from the Au foil. The spectra were taken by the SSD behind the gas ionization chamber with (red) and without (black) the P10 gas at 6.0×10^3 Pa. The initial energy of ^{16}O irradiated to the Au foil was set at 28.8 MeV. The difference of the leading edge positions between the two spectra signifies the energy loss due to the P10 gas filling the volume between the Mylar foil and the SSD. The distance between the Mylar foil and the SSD is 72 mm, while the length of the gas ionization chamber electrode is 50 mm. Therefore the gas ionization chamber approximately collects the ~ 70% (~ 50 /72) of the electrons produced along the trajectory. In this case, ΔE corresponds to the ~ 70% of the energy difference $\Delta E'$~ 5 MeV displayed in Fig. 3(b), and the rest energy loss is included in E_{others}. The energy difference $\Delta E'$ ~ 5 MeV is much larger than $\Delta E'$ ~ 3.6 MeV estimated by SRIM [18] with 6.0×10^3 Pa of the P10 gas pressure. The pressure estimated from SRIM is ~ 9.2×10^3 Pa. This discrepancy can be attributed to the uncertainty of SRIM and/or the underestimation of the P10 gas pressure due to the position of the diaphragm gauge (Fig. 1). We note, however, this uncertainty is still in a permissible range for the purpose of the determination of the elemental composition of metal oxynitrides.

Further energy calibration of the gas ionization chamber in detail is just time consuming as mentioned above. It is reasonable to estimate the response of the gas ionization chamber for recoils of other elements and with lower or higher energies from the stopping power table, if necessary. A comparison between experimental results and semi-empirical simulation based on the stopping power table validates this strategy for the elementary composition determination of the metal oxynitride thin films as discussed in the next subsection.

3.2. Performance test on $SrTaO_2N$

Figure 4(a) shows the ΔE-E histogram taken on the $SrTaO_2N$ film on $SrTiO_3$ substrate (t = 60 nm) with the developed detection system. The particle identification of each line seen in Fig. 4(a) was carried out by the comparison with the simulation using SIMNRA [20] shown in Fig. 4(b), and the results are indicated beside the lines. We can see that the simulation reproduced the experimental results. Apart from the scattered Cl particles, which form an intense line, we can see the recoils of light elements (O, N and C) and also of Ti and Sr. The small amount of C contamination probably implies the pileup of the hydrocarbon on the sample due to the not good enough vacuum pressure in the beam line (~ 10^{-4} Pa).

Figure 4(c) and 4(d) show the projections of O and N signals found in the

two-dimensional region of interest onto the E_{res} axis. Here the thicker film (t = 100 nm) was used for the convenience on the analysis. From the yield of O in the film and substrate and of N in the film, we can determine the composition ratio of the light elements in this system.

We employed following functions to fit the experimental spectra of O and N,

$$f_{O}(E_{res}) = \frac{C_1}{2}\left(\tanh\frac{E_{res}-E_{interface}}{w_{interface}} - \tanh\frac{E_{res}-E_{edge}}{w_{edge}}\right) + \frac{C_2}{2}\left(1-\tanh\frac{E_{res}-E_{interface}}{w_{interface}}\right),$$

$$f_{N}(E_{res}) = \frac{C_3}{2}\left(\tanh\frac{E_{res}-E_{interface}}{w_{interface}} - \tanh\frac{E_{res}-E_{edge}}{w_{edge}}\right).$$

Here E_{res} is a variable, E_{edge} and $E_{interface}$ are the fitting parameters corresponding to the channel numbers of the leading edge and interface for the O and N spectra, respectively. Then w_{edge} and $w_{interface}$ are the fitting parameters, which signify the energy broadening at the leading edge and interface, respectively. Finally, C_1, C_2 and C_3 are the fitting parameters, which represent the yields of O in the film, O in the substrate and N in the film, respectively. The results of fitting shown in Fig. 4(c) and 4(d) as circles and broken lines well reproduced the experiments.

Taking into account the stopping powers of the film and substrate materials for O and N and recoil cross sections, we derive the composition ratio from C_1, C_2 and C_3 as follows, N : O (film) : O (substrate) = 0.31 ± 0.06 O: 0.62 ± 0.05 : 1. This well agrees with the values 0.30 : 0.61 : 1 estimated from the stoichiometry, though the statistical errors are high due to the limited data acquisition time (several minutes). Thus the enough performance of ΔE-E telescope ERDA is validated to determine the ratio of N and O in the metal oxynitrides directly without any additional assumptions.

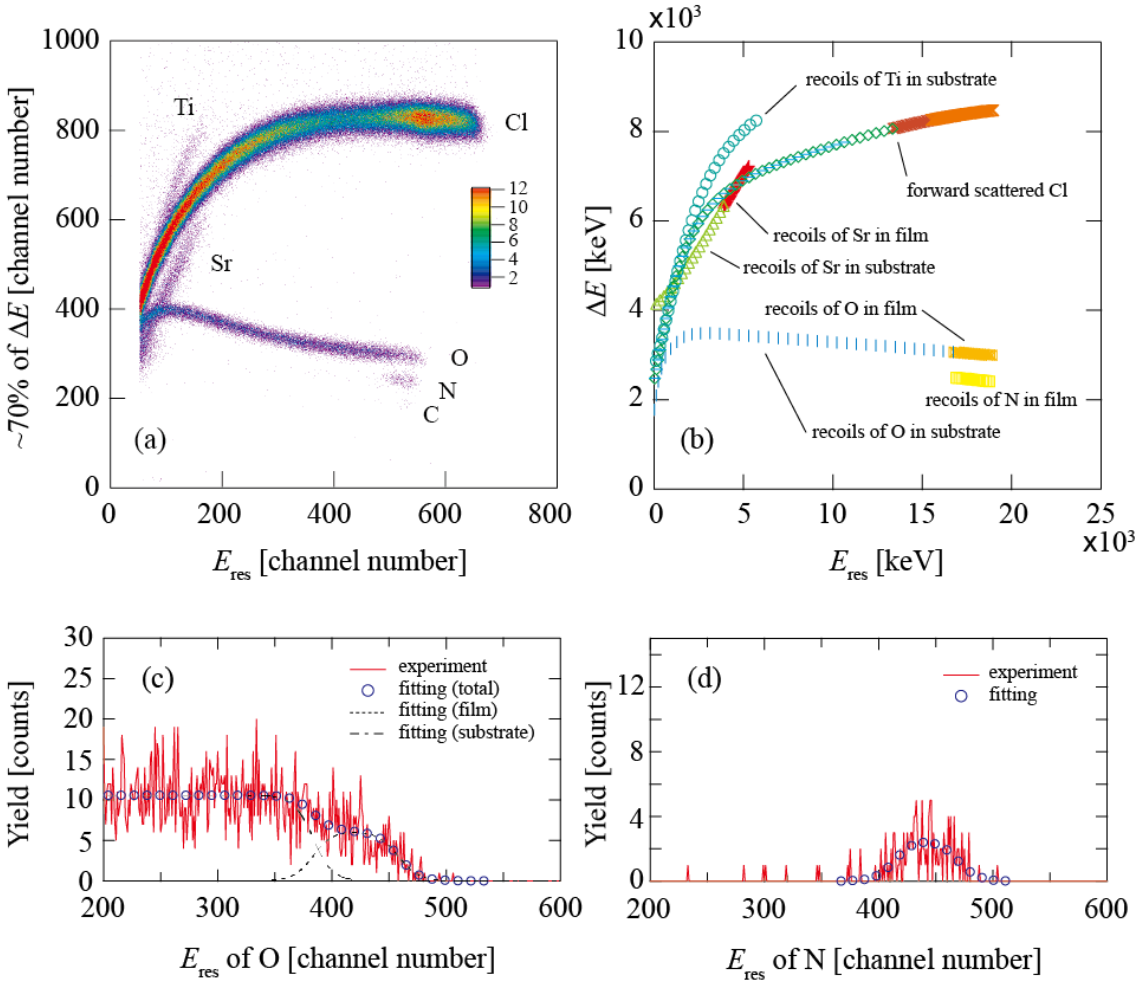

Fig. 4. (a) ΔE-E histogram taken on $SrTaO_2N/SrTiO_3$. (b) Semi-empirical simulation of ΔE-E distribution of $SrTaO_2N/SrTiO_3$ by SIMNRA code. (c) Spectrum of O recoils extracted from Fig. 4(a) and fitting results. (d) Spectrum of N recoils extracted from Fig. 4(b) and the fitting result.

3.3 Irradiation damage

The heavy ion beams often induce irradiation damage, such as sputtering, in samples [21-23]. Fig. 5 shows the variations of RBS yields of Sr, Ta and ERDA yields of O and N in a $SrTaO_xN_y$ film due to the 38.4 MeV $^{35}Cl^{7+}$ beam irradiation. Here beam dosage means the current measured on the sample with the digital current integrator ORTEC439 without the secondary electron suppresser, so that the real number of particles which hit the sample was smaller. From Fig. 5, the variation rates of Sr, Ta, O and N yields after the 250 μC beam dosage were estimated as +5 ± 5%, -6 ± 2%, -5 ± 5% and -10 ± 10%, respectively. This beam dosage usually corresponds to data acquisition time of about 80 minutes. To suppress the yield variation due to the irradiation damage, we change the irradiation position on samples every about 10 minutes.

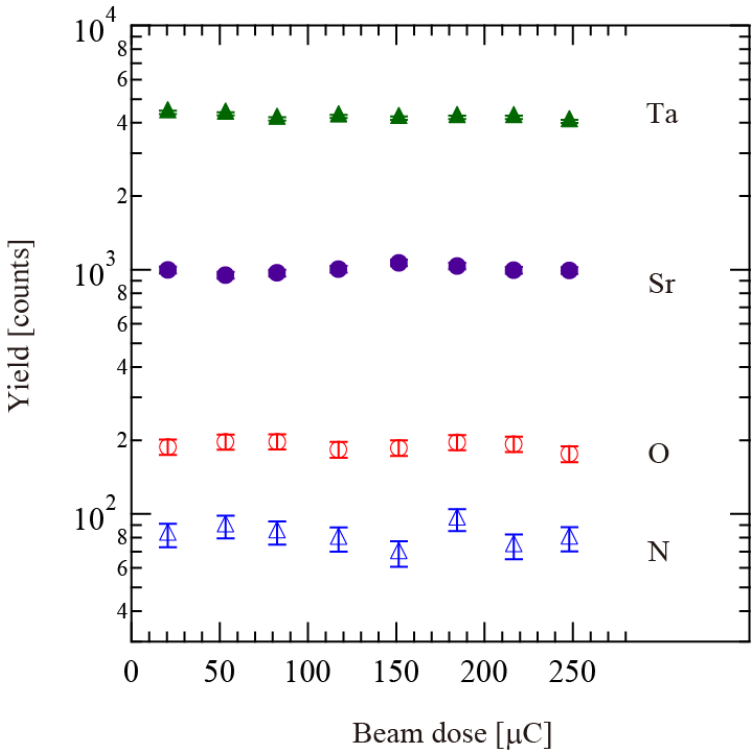

Fig. 5. Variations of the signal yields of each element including in $SrTaO_xN_y$ film with 38.4 MeV $^{35}Cl^{7+}$. The error bars are estimated from statistic errors. Each yield is normalized by beam dosage.

3.4 Application to samples with other light elements

Here we simply introduce the applications of the detector to other oxide, oxynitride, and oxyfluoride. Figure 6(a) ~ 6(d) show the ΔE-E histogram taken on the InO_xF_y film (t = 125 nm) on the Y:ZrO_2 substrate, the thick $LiTaO_3$ plate, the CoO_xN_y film (t = 90 nm) on the $MgAl_2O_4$ substrate and the SiO_2 film (t = 47 nm) on the Si wafer, respectively. These data were taken with the 39.2 MeV $^{35}Cl^{7+}$ beam except the Fig. 6(d) which was taken with the 38.4 MeV $^{35}Cl^{7+}$ beam. We can see that all the recoils of C, N, O, F, Li are well distinguished, indicating that the developed detector can quantify various metal-oxide-based materials including such light elements.

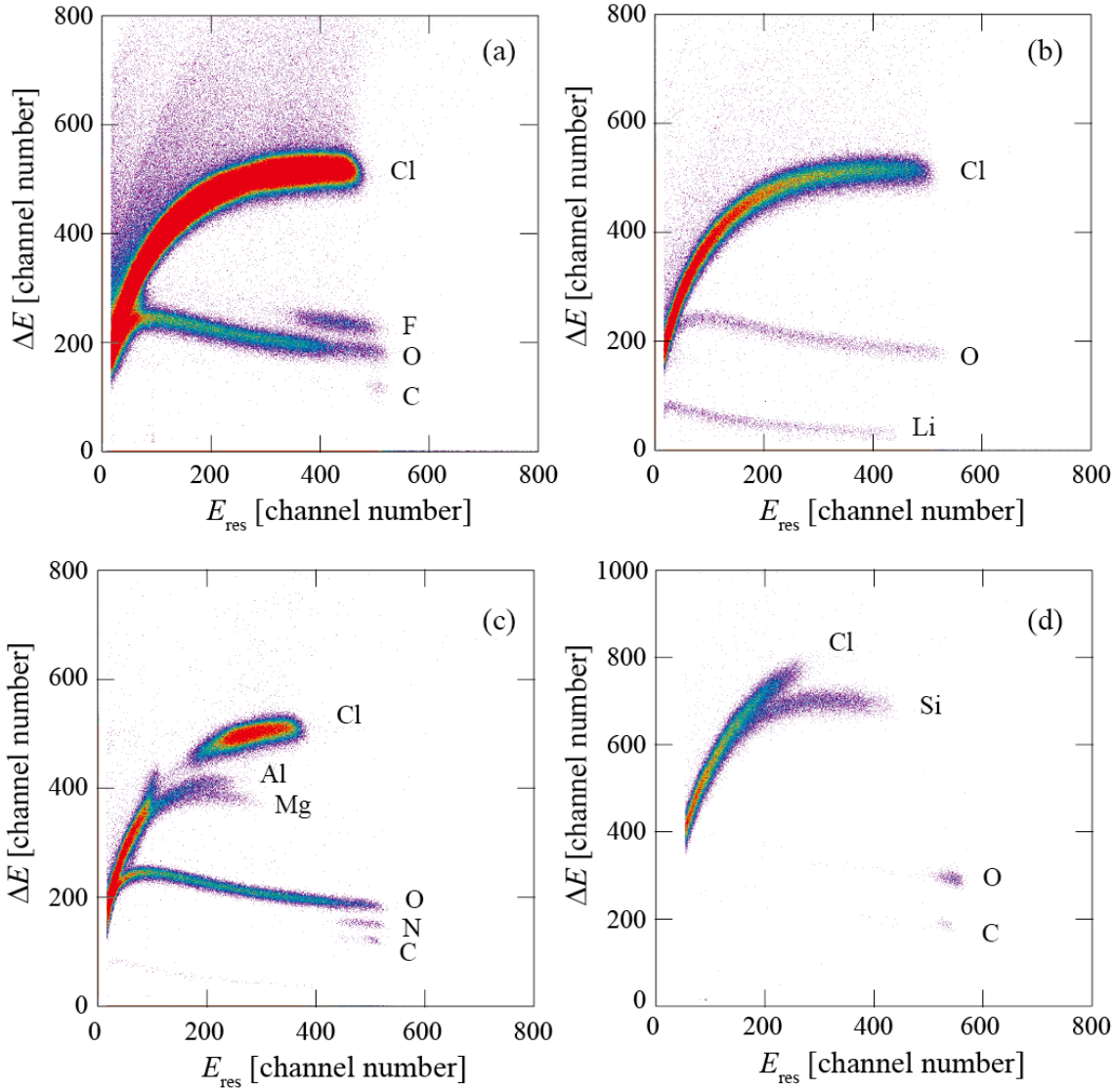

Fig. 6. ΔE-E histograms taken on (a) the InO_xF_y film (t = 125 nm) on the Y:ZrO_2 substrate, (b) the thick $LiTaO_3$ plate, (c) the CoO_xN_y film (t = 90 nm) on the $MgAl_2O_4$ substrate and (d) the SiO_2 film (t = 47 nm) on the Si wafer.

In the future works, we investigate also metal-oxide-based materials including hydrogen. Hydrogen is one of important dopants for metal-oxide-based materials [24-26]. Our current ERDA-RBS system, however, does not work effectively for hydrogen detection. To obtain the enough ΔE of hydrogen, the length of the electrodes should be longer [27] or the gas pressure should be higher [28] than those in our system. It seems to be not straightforward to precisely quantify hydrogen and oxygen in metal-oxide-based thin films simultaneously with common parameters in a single ΔE-E telescope ERDA system. Our solution is the combination with the conventional RBS-ERDA with 2.5 MeV $^4He^{2+}$ and the stopper foil [29,30]. The normalization between

the two methods, ΔE-E telescope ERDA and the conventional ERDA, can be easily done with the RBS yields of metal cations included in the thin film of oxides.

4. Conclusion

We designed and developed a simple and compact ΔE-E telescope ERDA system useful enough for the quantitative analysis of metal oxynitrides. The ~ 40 MeV $^{35}Cl^{7+}$ was employed as an incident beam. The developed detector expressed the expected performance on the $SrTaO_2N$ film (t = 60 and 100 nm) on the $SrTiO_3$ substrate. The detector successfully distinguished also Li, C and F.

Acknowledgement

The authors thank Dr. S. Okazaki, Dr. D. Oka, Mr. J. Takahashi, and Mr. M. Sano of the University of Tokyo for their assistance in sample preparation. The authors thank also Prof. K. Fukutani for the fruitful and critical discussions.

Reference

[1] A. Kobayashi, T. Ito, J. Ohta, M. Oshima, H. Fujioka, Phys. Status Solidi PRL **8**, (2014) 362.

[2] E. Aperathitis, M. Bender, V. Cimalla, G. Ecke, M. Modreau, J. Appl. Phys. **94** (2003) 1258.

[3] N.P. Barradas, N. Added, W.M. Arnoldbik, I. Bogdanović-Radović, W. Bohne, S. Cardoso, C. Danner, N. Dytlewski, P.P. Freitas, M. Jakšić, C. Jeynes, C. Krug, W.N. Lennard, S. Lindner, Ch. Linsmeier, Z. Medunić, P. Pelicon, R.P. Pezzi, C. Radtke, J. Röhrich, T. Sajavaara, T.D.M. Salgado, F.C. Stedile, M.H. Tabacniks, I. Vickridge, Nucl. Instr. and Meth. in Phys. Res. in Phys. Res. B **227** (2005) 397.

[4] A. Suzuki, Y. Hirose, D. Oka, S. Nakao, T. Fukumura, S. Ishii, K. Sasa, H. Matsuzaki, T. Hasegawa, Chem. Mater. **26** (2014) 976.

[5] D. Oka, Y. Hirose, H. Kamisaka, T. Fukumura, K. Sasa, S. Ishii, H. Matsuzaki, Y. Sato, Y. Ikuhara, T. Hasegawa, Scientific Reports **4** (2014) 4987.

[6] D. Logvinovich, A. Börger, M. Döbeli, S. G. Ebbinghaus, A. Reller, A. Weidenkaff, Progress in Solid Chemistry, **35** (2007) 281.

[7] I. Marozau, A. Shkabko, M. Döbeli, T. Lippert, M. Mallepill, C. W. Schneider, A. Weidenkaff, A. Wokaun, Acta Materialia **59** (2011) 7145.

[8] J. Jokinen, J. Keinonen, P. Tikkanen, A. Kuronen, T. Ahlgren, K. Nordlund, Nucl. Instr. and Meth. in Phys. in Phys. Res. B **119** (1996) 533.

[9] C. Kottler, M. Döbeli, F. Glaus, M. Suter, Nucl. Instr. and Meth. in Phys. in Phys. Res.

B **248** (2006) 155.

[10] Z. Siketić, I. Bogdanović Radvić, M. Jakšić, Nucl. Instr. and Meth. in Phys. in Phys. Res. B **266** (2008) 1328.

[11] M. Laitinen, M. Rossi, J. Julin, T. Sajavaara, Nucl. Instr. and Meth. in Phys. in Phys. Res. B **337** (2014) 55.

[12] M. Petrascu, I. Berceanu, I. Brancus, A. Buta, M. Duma, C. Grama, I. Lazar, I. Mihai, M. Petrovici, V. Simion, M. Mihaila, I. Ghita, Nucl. Instr. and Meth. in Phys. Res. in Phys. Res. B **4** (1984) 396.

[13] H. Matsuzaki, M. Tanikawa, K. Kobayashi, S. Hatori, Nucl. Instr. and Meth. in Phys. Res. B **172** (2000) 218.

[14] H. Oikawa, R. Akiyama, K. Kanazawa, S. Kuroda, I. Harayama, K. Nagashima, D. Sekiba, Y. Ashizawa, A. Tsukamoto, K. Nakagawa, N. Ota, Thin Solid Films **574** (2015) 110.

[15] S. Okazaki, Y. Hirose, S. Nakao, C. Yang, I. Harayama, D. Sekiba, T. Hasegawa, Thin Solid Films, **559** (2014) 96.

[16] J. Takahashi, Y. Hirose, D. Oka, S. Nakao, C. Yang, T. Fukumura, I. Harayama, D. Sekiba, T. Hasegawa, Appl. Phys. Lett. **107** (2015) 231906.

[17] H.H. Andersen, F. Besenbacher, P. Loftager, W. Möller, Phys. Rev. A 21 (1980) 1891.

[18] SRIM (http://www.srim.org/)

[19] Y. Zhang, H.J. Whitlow, Nucl. Instr. and Meth. in Phys. Res. B **190** (2002) 383.

[20] SIMNRA (http://home.rzg.mpg.de/~mam/)

[21] S. Sugden, C.J. Sofield, M.P. Murrell Nucl. Instr. and Meth. in Phys. Res. B **67** (1992) 569.

[22] S.R. Walker, J.A. Davies, J.S. Forster, S.G. Wallace, A.C. Kockelkoren Nucl. Instr. and Meth. in Phys. Res. B **136** (1998) 707.

[23] W.M. Arnoldbik, p.A. Zeijlmans van Emmichoven, F.H.P.M. Habraken, Phys. Rev. Lett. **94** (2005) 245504.

[24] Cetin Kilic, Alex Zunger, Appl. Phys. Lett. **81** (2002) 73.

[25] Takashi KOIDA, Hiroyuki FUJIWARA, and Michio KONDO , J. J. Appl. Phys. 46 (2007) 685

[26] Yoji Kobayashi, Olivier J. Hernandez, Tatsunori Sakaguchi, Takeshi Yajima, Thierry Roisnel, Yoshihiro Tsujimoto, Masaki Morita, Yasuto Noda, Yuuki Mogami, Atsushi Kitada, Masatoshi Ohkura, Saburo Hosokawa, Zhaofei Li, Katsuro Hayashi, Yoshihiro Kusano, Jung eun Kim, Naruki Tsuji, Akihiko Fujiwara, Yoshitaka Matsushita, Kazuyoshi Yoshimura, Kiyonori Takegoshi, Masashi Inoue, Mikio

Takano and Hiroshi Kageyama, Nature Mater. 11 (2012) 507.
[27] D. Pantelica, A. Isbasescu, F. Negoita, H. Petrascu, M. Petrascu, P. Ionescu, N. Scintee, Nucl. Instr. and Meth. in Phys. in Phys. Res. B **249** (2006) 504.
[28] A.M. Müller, M. Döbeli, M. Suter, H. A. Synal, Nucl. Instr. and Meth. in Phys. in Phys. Res. B **287** (2012) 94.
[29] D. Sekiba, M. Horikoshi, S. Abe, S. Ishii, J. Appl. Phys. **106** (2009) 114912.
[30] D. Sekiba, N. Takemoto, M. Okada, S. Ishii, T. Sakurai, K. Akimoto, Diamond Relat. Mater. **27-28** (2012) 60.